# Functional brain hubs and their test–retest reliability: A multiband resting-state functional MRI study

CrossMark

Xu-Hong Liao [a,b], Ming-Rui Xia [c], Ting Xu [d], Zheng-Jia Dai [c], Xiao-Yan Cao [a,b], Hai-Jing Niu [c], Xi-Nian Zuo [d], Yu-Feng Zang [a,b,*], Yong He [c,**]

[a] Center for Cognition and Brain Disorders, Hangzhou Normal University, Hangzhou, China
[b] Zhejiang Key Laboratory for Research in Assessment of Cognitive Impairments, Hangzhou, China
[c] State Key Laboratory of Cognitive Neuroscience and Learning & IDG/McGovern Institute for Brain Research, Beijing Normal University, Beijing, China
[d] Key Laboratory of Behavioral Science, Laboratory for Functional Connectome and Development, Magnetic Resonance Imaging Research Center, Institute of Psychology, Chinese Academy of Sciences, Beijing, China

## ARTICLE INFO

## ABSTRACT

Resting-state functional MRI (R-fMRI) has emerged as a promising neuroimaging technique used to identify global hubs of the human brain functional connectome. However, most R-fMRI studies on functional hubs mainly utilize traditional R-fMRI data with relatively low sampling rates (e.g., repetition time [TR] = 2 s). R-fMRI data scanned with higher sampling rates are important for the characterization of reliable functional connectomes because they can provide temporally complementary information about functional integration among brain regions and simultaneously reduce the effects of high frequency physiological noise. Here, we employed a publicly available multiband R-fMRI dataset with a sub-second sampling rate (TR = 645 ms) to identify global hubs in the human voxel-wise functional networks, and further examined their test–retest (TRT) reliability over scanning time. We showed that the functional hubs of human brain networks were mainly located at the default-mode regions (e.g., medial prefrontal and parietal cortex as well as the lateral parietal and temporal cortex) and the sensorimotor and visual cortex. These hub regions were highly anatomically distance-dependent, where short-range and long-range hubs were primarily located at the primary cortex and the multimodal association cortex, respectively. We found that most functional hubs exhibited fair to good TRT reliability using intraclass correlation coefficients. Interestingly, our analysis suggested that a 6-minute scan duration was able to reliably detect these functional hubs. Further comparison analysis revealed that these results were approximately consistent with those obtained using traditional R-fMRI scans of the same subjects with TR = 2500 ms, but several regions (e.g., lateral frontal cortex, paracentral lobule and anterior temporal lobe) exhibited different TRT reliability. Finally, we showed that several regions (including the medial/lateral prefrontal cortex and lateral temporal cortex) were identified as brain hubs in a high frequency band (0.2–0.3 Hz), which is beyond the frequency scope of traditional R-fMRI scans. Our results demonstrated the validity of multiband R-fMRI data to reliably detect functional hubs in the voxel-wise whole-brain networks, which motivated the acquisition of high temporal resolution R-fMRI data for the studies of human brain functional connectomes in healthy and diseased conditions.

## Introduction

Resting-state fMRI (R-fMRI) has emerged as a promising and powerful tool to explore intrinsic functional networks in the resting brain (i.e., functional connectome) (Biswal et al., 1995, 2010; Fox and Raichle, 2007; Kelly et al., 2012). Graph-theoretical analysis on resting-state brain networks has revealed a few global hubs with a disproportionally large number of functional connections (Achard et al., 2006; Buckner et al., 2009). The hub regions are mainly located at the medial prefrontal and parietal cortex as well as the lateral temporal and parietal cortex (Achard et al., 2006; Buckner et al., 2009; He et al., 2009; Liang et al., 2013; Tomasi and Volkow, 2011; Zuo et al., 2012). These spatially distributed hubs play essential roles in the interconnection of distributed functionally specified regions and in coordinating performance across the brain. Recently, several R-fMRI studies have demonstrated abnormalities in the hub configuration of brain functional networks in neuropsychiatric diseases (e.g., Alzheimer's disease, depression and schizophrenia) (Alexander-Bloch et al., 2013; Buckner et al., 2009; Wang et al., 2013; Zhang et al., 2011), indicating an important

association between the hub regions and a pathophysiological mechanism. Thus, the exploration of the spatial patterns of functional hubs is crucial for the understanding of the physiological basis for cognition and pathological behavior.

Until recently, most R-fMRI studies on functional hubs of brain networks have employed traditional fMRI data with relatively low sampling rates (e.g., repletion time [TR] = 2 s, $f_{sampling}$ = 0.5 Hz) in which the functional connections could be affected by the aliasing of high frequency respiratory (~0.3 Hz) and cardiac (~1 Hz) oscillations, even after temporal band-pass filtering (0.01–0.1 Hz) (Birn et al., 2006; van den Heuvel and Pol, 2010). Thus, the use of high sampling rate R-fMRI is of great importance because it is able to reduce the artificial correlations by preventing the aliasing of high frequency oscillations (Cordes et al., 2001; Lowe et al., 1998; van den Heuvel and Pol, 2010) and simultaneously provide additional temporal information about the functional integrity among brain regions (Feinberg et al., 2010; Smith et al., 2012; Zahneisen et al., 2011). Recently, several promising imaging techniques that enable whole-brain acquisition at sub-second temporal resolution have been proposed, including MR-encephalography (Zahneisen et al., 2011) and multiband echo planar imaging (Feinberg et al., 2010; Moeller et al., 2010). Using the multiband R-fMRI protocol, additional volumes of images can be acquired in the same scan duration without a significant loss in spatial resolution and the effect of non-neural oscillations (particularly the respiratory and cardiac signals) can be largely removed. However, whether multiband R-fMRI scans can effectively identify the spatial patterns of functional hubs in the brain remains largely unknown. Moreover, even though the functional hubs can be successfully detected, whether they can exhibit good test–retest (TRT) reliability is still unclear.

TRT reliable measurements (e.g., network metrics) are important for the inference of convincing conclusions, and serve as potential clinical biomarkers. Recently, increasing attention has been given to the TRT reliability studies using R-fMRI data, particularly in the assessment of various network metrics (Braun et al., 2012; Guo et al., 2012; Liang et al., 2012; Wang et al., 2011; Zuo et al., 2012). The TRT reliability of the network metrics may be potentially affected by several factors, such as acquisition parameters (Van Dijk et al., 2010; Whitlow et al., 2011) and fluctuations of conscious states (Greicius et al., 2008; Horovitz et al., 2008). The selection of different preprocessing strategies (e.g., global signal removal) is another important factor that affects TRT reliability of network metrics and has also been previously discussed in detail (Braun et al., 2012; Guo et al., 2012; Liang et al., 2012; Schwarz and McGonigle, 2011). For multiband R-fMRI data, the TRT reliability of regional functional homogeneity has been systematically investigated in a previous report (Zuo et al., 2013); however, the TRT reliability of network metrics for whole-brain functional networks still remains to be elucidated.

In the present study, we analyzed a recently published public multiband test–retest R-fMRI dataset (TR = 645 ms), which included 11 participants who were each scanned twice around one week apart. To address the above-mentioned questions, we employed this sub-second multiband R-fMRI dataset and the measure of nodal degree centrality to detect functional hubs in the voxel-wise functional networks, and further assessed their TRT reliability using intraclass correlation coefficients. Next, we investigated the effect of scan duration and global signals on TRT reliability of degree because these factors are relevant to the TRT analysis of traditional fMRI scans (Braun et al., 2012; Guo et al., 2012; Liang et al., 2012; Van Dijk et al., 2010; Whitlow et al., 2011). Furthermore, we compared the functional hubs and their TRT reliability with those derived from traditional R-fMRI data (TR = 2500 ms, $f_{sampling}$ =0.4 Hz) of the same subjects. Finally, using the sub-second multiband R-fMRI data, we explored the functional hubs and their TRT reliability in a high frequency band (0.2–0.3 Hz), which is beyond the frequency scope of traditional R-fMRI scans.

## Materials and methods

### Subjects

We used the multiband imaging test–retest pilot dataset that is publicly available from INDI (http://fcon_1000.projects.nitrc.org/indi/pro/eNKI_RS_TRT/FrontPage.html), consisting of 24 subjects (age: 34.4 ± 12.9, 6 females). The phenotype information of these subjects was provided in detail (see Table S1 in Supplementary materials). Recently, this dataset has been used to examine the TRT reliability of regional functional homogeneity in the human brain (Zuo et al., 2013). In this study, in order to exclude the potential effects of confounding health issues, we first discarded the data of 7 subjects with current/historical psychiatric disorders, and discarded 4 subjects without diagnostic information. The unique subject identification numbers for these 11 subjects were marked in Table S1. Then we further discarded the data of 1 healthy subject with obvious brain atrophy (subject 21001) and 1 healthy subject with excessive head motion (subject 3795193, see Data preprocessing). Finally, the data of the remaining 11 healthy subjects were analyzed in this study.

### Data acquisition

All subjects were scanned on a Siemens Trio 3.0 T scanner. For each subject, the R-fMRI scans were performed twice (session 1 and session 2), around one week apart, using three different sampling rates (see below for details). During the resting-state scans, the subjects were instructed to keep their eyes open and to look at the fixation cross, but not to stare or strain their eyes.

For each session, R-fMRI data were acquired using three scanning protocols: (1) Multiband R-fMRI (mR-fMRI) scan with TR = 645 ms: time echo = 30 ms; flip angle = 60°; 40 slices, multiband accelerate factor = 4; matrix = 74 × 74; field of view = 222 × 222 mm²; voxel size = 3 × 3 × 3 mm³; scan duration ~10 min (i.e., 900 volumes). Due to a malfunction in the temporary storage transfer protocol, the last (900th) volume was missing in 15 subjects. Thus, we removed the last volume (900th) from the dataset so that each subject would have the same number of volumes (n = 899); (2) mR-fMRI scan with TR = 1400 ms: time echo = 30 ms; flip angle = 65°; 64 slices, multiband accelerate factor = 4; matrix = 112 × 112; field of view = 224 × 224 mm²; voxel size = 2 × 2 × 2 mm³; scan duration ~10 min (i.e., 404 volumes); and (3) Traditional R-fMRI (tR-fMRI) using common echo-planar imaging sequence with TR = 2500 ms: time echo = 30 ms; flip angle = 80°; 38 slices; matrix = 72 × 72; field of view = 216 × 216 mm²; voxel size = 3 × 3 × 3 mm³; scan duration = 5 min (i.e., 120 volumes). In addition, a high-resolution T1-weighted anatomical image, task-based fMRI images and diffusion tensor imaging data were also obtained for each subject. In this study, we just employed the test–retest mR-fMRI data with TR = 645 ms, which provided the sub-second temporal resolution for the functional network analysis. The repeated tR-fMRI data (TR = 2500 ms) with the same spatial resolution were also used for reference and complementary analysis.

### Data preprocessing

All of the R-fMRI data were preprocessed using Statistical Parametric Mapping (SPM8, http://www.fil.ion.ucl.ac.uk/spm) and Data Processing Assistant for Resting-State fMRI (DPARSF) (Yan and Zang, 2010). Briefly, the volumes in the first 10 s were discarded (16 volumes for mR-fMRI and 4 volumes for tR-fMRI) for signal equilibrium. The remaining data were corrected for head motion, and one subject (subject 3795193) was excluded from further analysis due to excess head motion (rotation > 3°). These data were then spatially normalized to the Montreal Neurological Institute (MNI) space and resampled to 3-mm isotropic voxels. Next, the linear trend of the data was removed, and temporal band-pass filtering (0.01–0.1 Hz) was performed to reduce the effects

of low-frequency drift and high-frequency physiological noise (Biswal et al., 1995; Lowe et al., 1998). Finally, six head motion parameters and three potential nuisance signals, including the cerebrospinal fluid, white matter and global signals, were removed from the time course of each voxel using multiple linear regression (Fox et al., 2005). We did not perform spatial smoothing, because spatial smoothing prior to the network construction might introduce artificial local correlations to the adjacent voxels.

*Network analysis*

Given that some regions on the top of the brain and at the bottom of the cerebellum were not fully covered during the R-fMRI scans, we generated a group gray matter mask (gray matter probability ≥ 0.2) that included the cortical and subcortical regions ($N = 44,401$ voxels), which were present across all subjects in the repeated R-fMRI scans. The subsequent network analysis was performed within this mask.

*Network construction*

For a voxel-wise functional network, the functional connectivity between two voxels (nodes) was estimated using the temporal similarity between their BOLD signals. Initially, the time courses of all voxels were extracted from the preprocessed R-fMRI data. Next, a symmetric correlation matrix $R = [r_{ij}]$ was generated, where $r_{ij}$ represents the Pearson's correlation coefficient between the BOLD signals of the voxels $i$ and $j$. Finally, a threshold $r_{th}$ was applied to estimate whether a connection existed, and the network sparsity was calculated as the ratio of the total number of connections in the network to the maximum possible number of connections. Both the binary and weighted networks were generated for each subject, and different correlation threshold values ($r_{th} = 0.1, 0.2, 0.3, 0.4$) were considered. A binary adjacency matrix representing the functional network was defined as

$$a_{ij} = \begin{cases} 0, & r_{ij} \leq r_{th} \\ 1, & r_{ij} > r_{th} \end{cases}. \tag{1}$$

Similarly, the weighted adjacency matrix was also considered as follows

$$a_{ij} = \begin{cases} 0, & r_{ij} \leq r_{th} \\ z_{ij}, & r_{ij} > r_{th} \end{cases}, \tag{2}$$

where $z_{ij}$ indicates the Fisher's r-to-z transformation (Zar, 1996) of element $r_{ij}$ to improve the normality of the correlation distribution. Given the same threshold $r_{th}$, the network sparsity was identical for both binary and weighted functional networks, as it only took into account the number of connections regardless of the weight. Importantly, we just focused on the connections with positive correlations because the physiological basis of the negative correlations was ambiguous (Fox et al., 2009; Murphy et al., 2009; Weissenbacher et al., 2009).

*Degree centrality*

Degree centrality is one of the most popular graphical measures used to identify global hubs in the brain (Bullmore and Sporns, 2009; Rubinov and Sporns, 2010). In graph theory, the degree $k$ for voxel $i$ in the network is defined as (Dai et al., 2012; Opsahl et al., 2010; Rubinov and Sporns, 2010)

$$k_i = \frac{1}{N-1} \sum_{j \neq i} a_{ij}, \tag{3}$$

where $N$ is the total number of voxels in the group gray matter mask. The degree centrality of a voxel indicates its average functional connectivity strength with all of the other voxels, and characterizes its influence in the network. According to Eqs. (1) (2) and (3), we computed both the binary and weighted degree centralities of the brain networks.

*Distance-dependent degree centrality maps*

The functional connections between different regions are closely associated with their anatomical locations (Achard et al., 2006; Liang et al., 2013; Salvador et al., 2005a; Sepulcre et al., 2010). To explore the effects of anatomical distance on functional connections, the three-dimensional anatomical distance between every pair of voxels ($i$ and $j$) was approximated using the Euclidean distance:

$$D_{ij} = \sqrt{\left(x_i - x_j\right)^2 + \left(y_i - y_j\right)^2 + \left(z_i - z_j\right)^2}, \tag{4}$$

where ($x_i, y_i, z_i$) and ($x_j, y_j, z_j$) are stereotaxic coordinates for voxels $i$ and $j$, respectively, in MNI space. The functional connections of each voxel were classified as either short-range or long-range with a distance criterion of 75 mm (Achard et al., 2006). Consequently, the short-range and long-range degree centralities were computed as the average functional connection strength of a voxel with other voxels in different spatial ranges.

Using the combination of network types and distance factors, we generated six types of degree maps for each subject, including binary overall degree (boDeg), binary short-range degree (bsDeg), binary long-range degree (blDeg), weighted overall degree (woDeg), weighted short-range degree (wsDeg) and weighted long-rang degree (wlDeg) maps. Prior to statistical analysis, all of the individual degree centrality maps were spatially smoothed using SPM8 with a Gaussian smoothing kernel (FWHM = 6 mm).

*Identification of global hubs*

For each session, we generated six group-level voxel-wise degree centrality maps by averaging the individual degree maps across all of the subjects (i.e., boDeg, bsDeg, blDeg, woDeg, wsDeg and wlDeg). For each group-level map, the degree values were standardized by converting into z-scores as follows (Buckner et al., 2009):

$$z_i = \frac{k_i - \bar{k}}{\sigma}, i = 1, 2, ..., N. \tag{5}$$

In the formula, $\bar{k}$ represents the mean degree across the brain, and $\sigma$ represents the corresponding standard deviation. Regions displaying relatively strong functional connectivity ($z_i \geq 1$) were identified as functional hubs. The spatial similarity of the functional hubs in different conditions was evaluated using Pearson's correlation coefficient across voxels. Because the neighbor voxels were dependent due to physiological correlations and the spatial processing, the effective degree of freedom in the across-voxel correlation analysis was corrected to estimate the p-values (Liang et al., 2013; Xiong et al., 2004).

*Test–retest reliability of degree centrality*

To further evaluate the TRT reliability of the voxel degree between the two sessions, a measurement of the intraclass correlation coefficient (ICC) was employed. Given a voxel, the individual degree values of all subjects in the two sessions were first analyzed using one-way ANOVA analysis with random subject effects. Then an ICC value was calculated according to the equation (Shrout and Fleiss, 1979)

$$ICC = \frac{BMS - WMS}{BMS + (m-1)WMS}, \tag{6}$$

where $BMS$ ($WMS$) represents the between-subject (within-subject) mean square and $m$ represents the number of repeated measurements of the voxel degree (here, $m = 2$). We calculated the ICC value for each voxel and generated the ICC map for each type of degree centrality (boDeg, bsDeg, blDeg, woDeg, wsDeg and wlDeg). Next, the TRT reliability of the degree was assessed in a voxel-wise manner with the classifying criteria of ICC values (Sampat et al., 2006): less than 0.4 indicated low reliability; 0.4 to 0.6 indicated fair reliability; 0.6 to 0.75 indicated

good reliability and 0.75 to 1.0 indicated excellent reliability. For mR-fMRI data, to further assess the regional variability of TRT reliability, we utilized a prior functional parcellation of cerebrum (Yeo et al., 2011), and calculated the mean ICC values and their standard deviations within seven subnetworks (visual, somatomotor, dorsal attention, ventral attention, limbic, frontoparietal and default-mode), respectively.

*Influence of two factors: scan duration and global signals*

*Effects of scan duration on TRT reliability*

Compared with the tR-fMRI technique, the mR-fMRI technique can acquire more volumes and additional temporal information within the same scan duration (Feinberg et al., 2010; Smith et al., 2012). Nonetheless, the signal-to-noise ratio of the images might also be reduced due to the short acquisition time of each volume (Feinberg et al., 2010). To investigate the effect of the scan duration on the patterns of functional hubs, spatially normalized mR-fMRI data from each session were truncated into 9 bins with the $i^{th}$ bin containing the first $i$ minutes of signal acquisition. Thus 9 bins of data with a scan duration ranging from 1 min to 9 min were generated for each subject. Next, we performed a linear detrend, temporal filtering and nuisance regression on each bin of data in the same manner as those in Data preprocessing. For each bin of data, we generated individual degree maps in six cases (i.e., boDeg, bsDeg, blDeg, woDeg, wsDeg and wlDeg) again and evaluated the TRT reliability of the degree. To assess the influence of scan duration in tR-fMRI, similar methods were also applied to the entire scan of tR-fMRI data in both sessions, with a scan duration ranging from 1 min to 5 min.

*Effects of global signals on functional hubs and TRT reliability*

The physiological basis of the global signals is still unclear (Fox et al., 2009; Murphy et al., 2009). In recent years there has been an ongoing debate on global signal removal in the preprocessing (Braun et al., 2012; Fox et al., 2009; Guo et al., 2012; Liang et al., 2012; Murphy et al., 2009; Weissenbacher et al., 2009). To investigate the effects of global signals on functional hubs and their TRT reliability, we also performed a network analysis without global signal removal (GSR) on both mR-fMRI and tR-fMRI data.

*Comparisons with different sampling rates*

Compared with tR-fMRI, mR-fMRI demonstrated a higher temporal resolution by improving the sampling rates. To explore the effect of the sampling rates, functional hub detection and TRT reliability analysis were also performed on the tR-fMRI data of the same subjects with TR = 2500 ms using the following procedure: (i) To determine whether the regions exhibited significantly different degree values between mR-fMRI and tR-fMRI, a voxel-wise paired $t$-test was separately performed on the degree maps across subjects for each session. (ii) To further explore the differences in TRT reliability of the voxel degree between mR-fMRI and tR-fMRI, a direct comparison of the TRT reliability maps was performed by subtracting the tR-fMRI maps from the mR-fMRI maps. Importantly, to ensure comparability of results with different sampling rates, the R-fMRI data within the same scan duration (i.e., scan duration = 290 s, which corresponded to the total 116 volumes for tR-fMRI and first 450 volumes for mR-fMRI) were used in the quantitative comparisons. (iii) To exclude scanning order effects on the degree difference, the order effects during a single scan were further examined. The single mR-fMRI scan (i.e., 883 volumes) was divided into two sections with approximately equal scan duration: the first half scan (442 volumes) and the second half scan (441 volumes). In each session, individual degree maps were separately generated for two sections, and regions exhibiting significantly different degree values between the two half scans were identified by a voxel-wise paired $t$-test across subjects. All of the resulting t-maps were corrected for multiple comparisons within the group mask using a Monte Carlo simulation (AlphaSim by B. Douglas Ward) at a corrected $p < 0.05$ (uncorrected

$p < 0.05$, cluster size > 131 voxels). (iv) Using the whole scan of the mR-fMRI data, we explored the functional hubs and their TRT reliability in a higher frequency band (0.2–0.3 Hz) that was undetectable using the tR-fMRI dataset with TR = 2500 ms. To obtain the mR-fMRI data at this frequency range, we applied temporal band-pass filtering (0.2–0.3 Hz) during the data preprocessing.

*Head motion analysis*

Recent R-fMRI studies have reported that head motion induces spurious and systematic functional correlations despite performing nuisance regression with head motion parameters (Power et al., 2012; Satterthwaite et al., 2013; Van Dijk et al., 2012). To further assess the effects of transient head motion, we removed volumes with large instantaneous head motion from both the mR-fMRI and tR-fMRI data (Power et al., 2012). We scrubbed the volumes with framewise displacement (FD) above 0.5 mm and their adjacent volumes (1 back and 2 forward) for each subject. Subjects who retained more than 80% of the original data in both sessions were included in the analysis. We then recalculated the individual degree maps and assessed their TRT reliability for both mR-fMRI and tR-fMRI data.

## Results

Using the mR-fMRI data, we generated both binary and weighted voxel-wise whole-brain functional networks and further investigated the functional hubs and their TRT reliability. The results were highly similar, not dependent on the binary or weighted approaches or different correlation thresholds considered ($r_{th}$ = 0.1, 0.2, 0.3, 0.4). For this reason, we mainly reported the results in weighted brain networks thresholded with $r_{th}$ = 0.2. The other results from the binary and weighted networks with different thresholds can be found in the Supplementary materials.

*Functional hubs in whole-brain functional networks*

For the mR-fMRI data, voxel-wise functional networks were generated for each subject, which had sparse functional connections (mean sparsity < 0.2, Table 1), and no significant difference was observed between two sessions. For each session, we generated group-level voxel-wise degree centrality maps in three cases (woDeg, wsDeg and wlDeg). The functional hubs (Figs. 1A and B) were spatially non-homogeneous across regions, whereas their spatial patterns were highly similar between the two sessions. Quantitative spatial correlation analysis (Pearson's correlation across voxels) revealed high correlation coefficients between the maps in the two sessions (Fig. 1C, session 1 vs. session 2, woDeg: r = 0.96; wsDeg: r = 0.97; wlDeg: r = 0.97, all ps < 0.00001, df$_{eff}$s = 5548). In the weighted overall degree map (Figs. 1A and B, woDeg), the functional hubs were predominantly

**Table 1**
Sparsity of voxel-wise human brain functional networks ($r_{th}$ = 0.2, with GSR).

| Scan duration (minutes) | Data type | Sparsity (mean ± std) | | p value |
|---|---|---|---|---|
| | | Session 1 | Session 2 | |
| ~10 | mR-fMRI | 0.123 ± 0.024 | 0.137 ± 0.020 | 0.114 |
| ~5 | mR-fMRI | 0.155 ± 0.019 | 0.173 ± 0.014 | 0.026* |
| ~5 | tR-fMRI | 0.157 ± 0.014 | 0.179 ± 0.031 | 0.004** |

The mean network sparsity for each session was calculated by averaging individual network sparsity across 11 subjects. The differences of the network sparsity between two sessions were assessed by paired t-tests, indicated by one star (p < 0.05) or two stars (p < 0.01). In addition, no significant difference was observed in the network sparsity between different sampling rates during the same scan duration (~5 min), with p = 0.811 for session 1 and p = 0.531 for session 2.
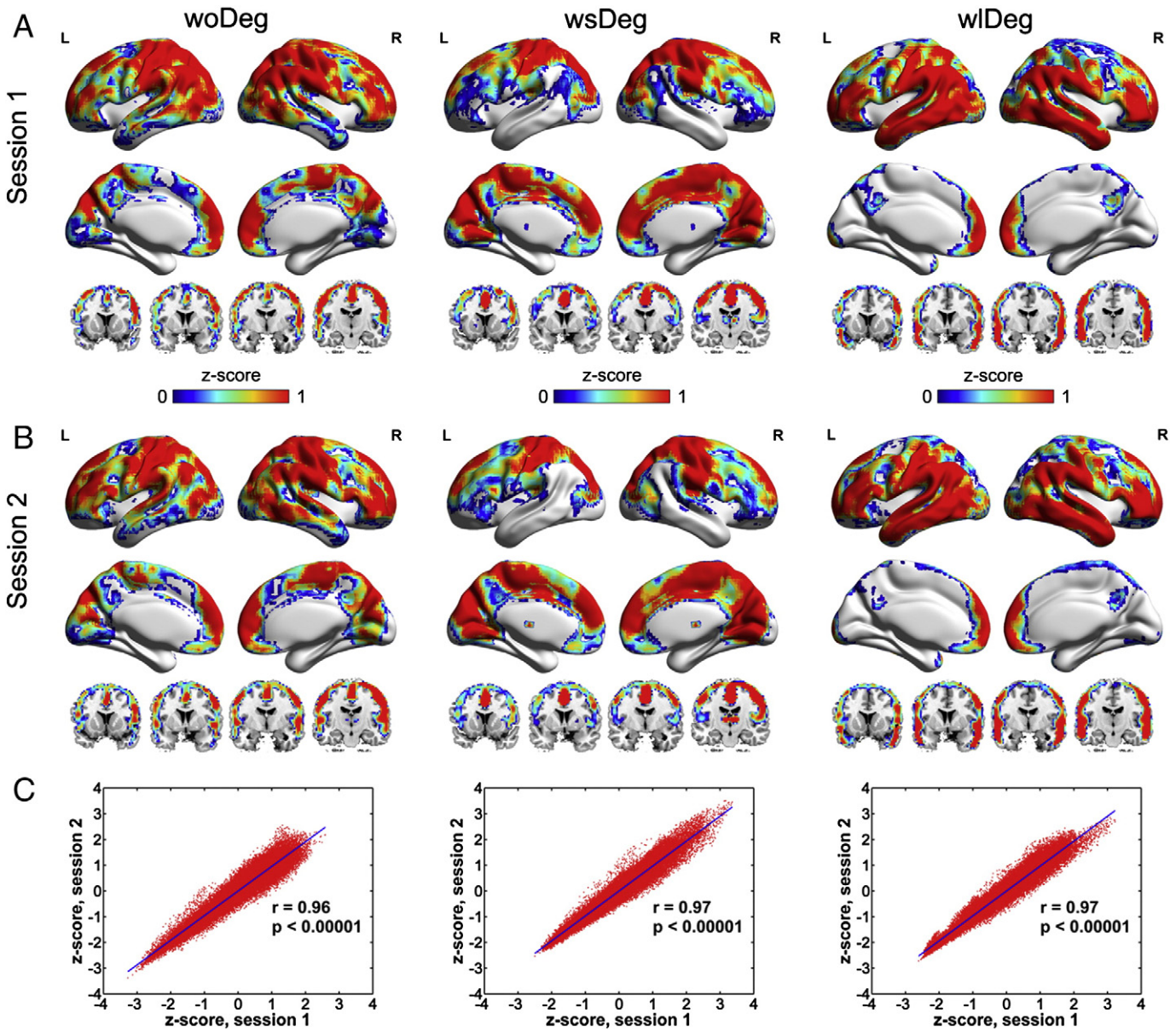
**Fig. 1.** Group-level voxel-wise degree centrality maps on the basis of mR-fMRI data and their consistency across sessions. A, spatial patterns of functional hubs in session 1. B, spatial patterns of functional hubs in session 2. C, spatial similarity of functional hubs between the two sessions. Three types of degree centralities (woDeg, wsDeg and wlDeg) were considered to explore the effect of anatomical distance, and all of the degree values were converted into z-scores to identify the global hubs. Only voxels with z-scores above zero are displayed in the maps. These hemispheric surfaces were visualized using BrainNet Viewer (http://www.nitrc.org/projects/bnv/, Xia et al., 2013), and the subcortical regions are displayed in 4 coronal slices with y coordinates from 13 mm to −14 mm with 9 mm space, same hereinafter.

located at several default-mode regions (e.g., posterior cingulate gyrus, medial prefrontal cortex and inferior parietal cortex), superior parietal lobule, inferior frontal gyrus, the sensorimotor cortex and visual regions. Moreover, these functional hubs were distance-dependent. Short-range hubs were mainly located at the sensorimotor cortex, visual regions, thalamus, superior parietal lobule and medial frontal cortex (Figs. 1A and B, wsDeg). In contrast, the long-range hubs were primarily located at the medial prefrontal and parietal cortex as well as the lateral frontal, temporal and parietal cortex (Figs. 1A and B, wlDeg). Similar functional hub configurations were identified in both binary and weighted brain networks derived at different thresholds (Fig. S1), which were elucidated by quantitative spatial correlation analysis. Functional hubs in the weighted networks derived at other thresholds ($r_{th} = 0.1$, 0.3, 0.4) are displayed in Fig. S2, and we observed that the posterior cingulate gyrus/precuneus became more conspicuous as the threshold increased.

### Test–retest reliability of degree centrality

For each type of degree, the TRT reliability at each voxel was evaluated by an ICC value. The resulting reliability maps were spatially non-homogeneous across the brain in all cases (see Fig. 2A, woDeg, wsDeg and wlDeg). Briefly, normalized histograms of ICC values across the brain are displayed in Fig. 2B, with a mean ICC value around 0.31 for woDeg, 0.34 for wsDeg and 0.33 for wlDeg. For the category of ICC values, approximately 41.6% of the voxels exhibited fair to excellent reliability in the overall networks (fair: around 26.7%; good: around 12.4%; excellent: around 2.5%), and this proportion changed to 47.5% and 42.3% for short-range and long-range degree centralities, respectively. Specifically, several hub regions, including some default-mode areas (e.g., precuneus, ventromedial prefrontal cortex and inferior parietal lobule), inferior frontal gyrus and the sensorimotor cortex, showed fair to good TRT reliability (ICC > 0.4), independent of the degree type.
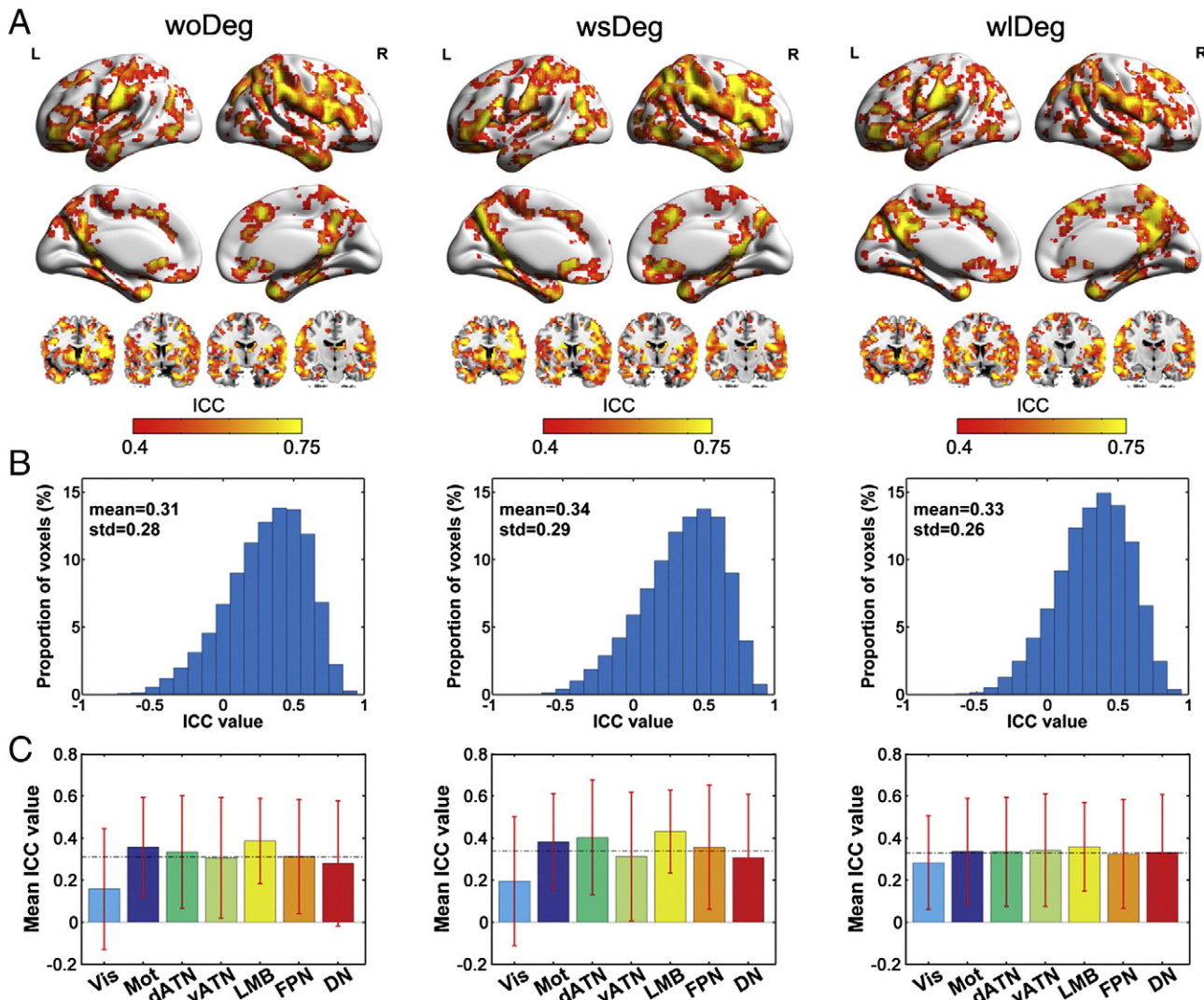
Fig. 2. TRT reliability for three types of degree centralities (woDeg, wsDeg and wlDeg) on the basis of repeated mR-fMRI scans. A, TRT reliability maps of degree. Only voxels with ICC values above 0.4 are displayed, same hereinafter. B, normalized histograms of voxel ICC values across the brain. C, mean ICC values and their standard deviations within seven specific subnetworks obtained from a prior parcellation of the cerebrum (Yeo et al., 2011). The dash-dotted line indicates the mean ICC value across the whole brain. Seven colors indicate different subnetworks, including the visual (Vis), somatomotor (Mot), dorsal attention (dATN), ventral attention (vATN), limbic (LMB), frontoparietal (FPN) and default (DN) networks.

Besides, some non-hub subcortical regions (e.g., caudate nuclei, putamen, insula and hippocampus) also exhibited fair to good reliability, irrespective of the degree type. Regional variability of TRT reliability was also assessed in Fig. 2C within seven specific subnetworks (visual, somatomotor, dorsal attention, ventral attention, limbic, frontoparietal and default-mode) (Yeo et al., 2011), with large standard deviations identified. Similar ICC values were found in different subnetworks, except the visual subnetwork. The hub region of the cuneus exhibited poor TRT reliability (mean ICC < 0.2) in woDeg and wsDeg, which could be due to the uncontrolled eye movements during the resting-state scans. Similar spatial patterns were found in the reliability maps of weighted networks derived at other thresholds (Fig. S3), with high spatial correlation coefficients (e.g., woDeg, $r_{th} = 0.1$ vs. 0.2: r = 0.98; $r_{th} = 0.3$ vs. 0.2: r = 0.97; $r_{th} = 0.4$ vs. 0.2: r = 0.86, all ps < 0.00001, $df_{eff}s = 5548$).

### Influence of scan duration on TRT reliability of degree centrality

For the weighted overall degree (i.e., woDeg), the voxel-wise TRT reliability maps are illustrated in Fig. 3A for each bin of mR-fMRI data, with a scan duration ranging from 1 min to 9 min. To get more details on the

changes of TRT reliability across time, the normalized frequency polygons of ICC values (Fig. 3B) across the brain and their mean values (Fig. 3C) were displayed for different scan durations separately. Similar trends were observed for the three types of degree (woDeg, wsDeg and wlDeg). In general, we found that the distribution profile of the ICC values considerably shifted to the right as the scan duration increased. Nonetheless, the increasing trend of mean ICC values was slightly fluctuating during the first 5 min, and became inconspicuous after 6 min, suggesting that the TRT reliability of degree centrality tended to be stable after 6 min. This phenomenon was also observed in the TRT reliability maps of the short-range and long-range degree centralities (i.e., wsDeg and wlDeg, Fig. S4). Similar changing trends were found for TRT reliability maps derived from tR-fMRI data (Fig. S5). For the tR-fMRI data, the TRT reliability of the degree increased with fluctuations when the scan duration increased from 1 min to 5 min.

### Influence of global signals on functional hubs

To explore the influence of global signals, we constructed functional networks on the basis of the entire scan of mR-fMRI data without GSR. The mean network sparsity across subjects was $0.331 \pm 0.127$ and
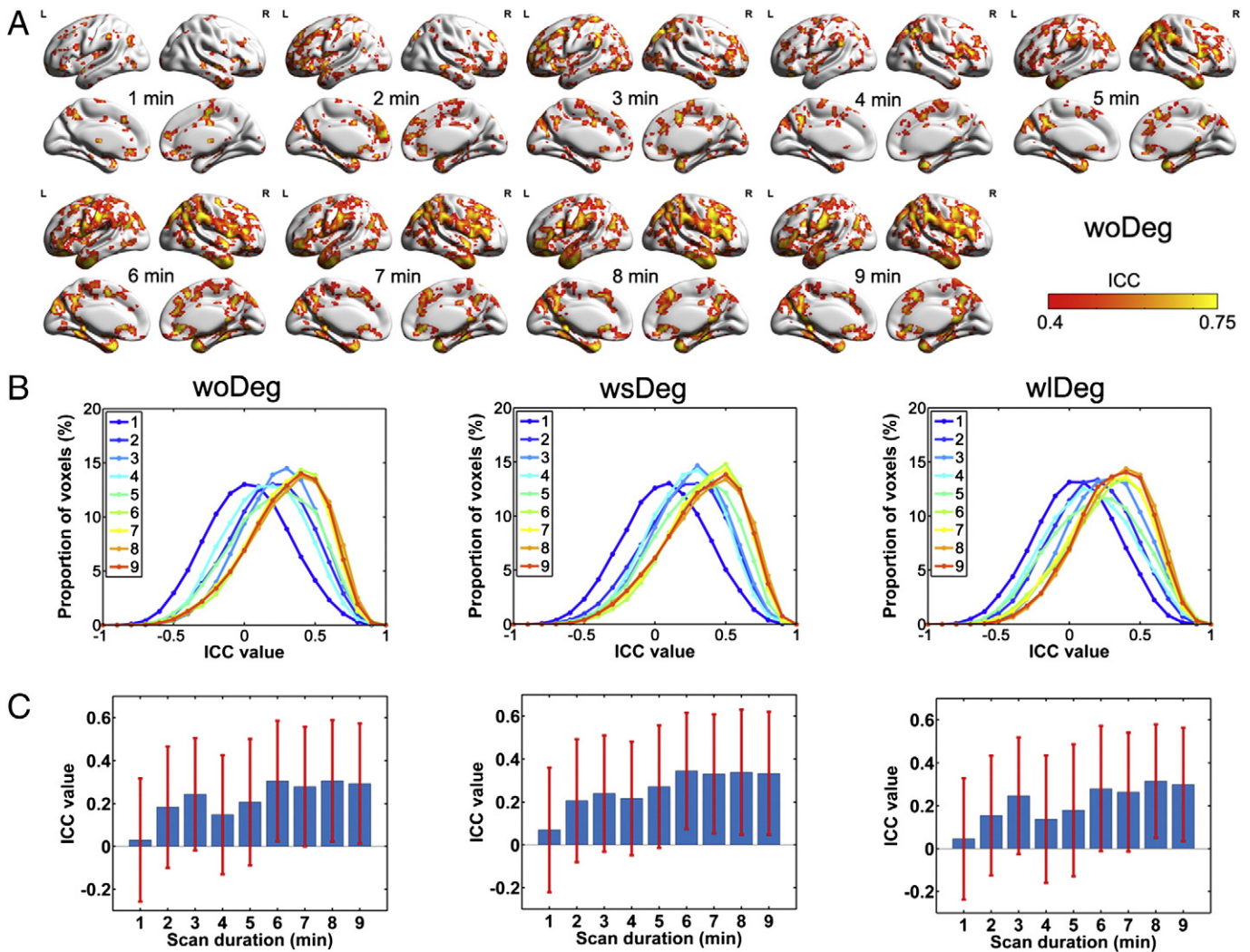
**Fig. 3.** Influence of scan duration on TRT reliability of degree derived from mR-fMRI data. A, TRT reliability maps of woDeg with increasing scan duration ranging from 1 min to 9 min. B, normalized frequency polygons of voxel ICC values across the brain for different scan durations. C, mean ICC values and their standard deviations across the brain for different scan durations. For three types of degree centralities, the distribution profile and the mean ICC values tended to be stable after 6 min. Only the TRT reliability maps for woDeg are illustrated here. The results for wsDeg and wlDeg can be found in the Supplementary materials (Fig. S4).

$0.379 \pm 0.162$ for session 1 and session 2, respectively, which was significantly larger than that derived with GSR (p < 0.001 for both sessions). The spatial patterns of the functional hubs in session 1 and session 2 are displayed in Figs. 4A and S6A, respectively. Compared with the results with GSR (Fig. 1), the functional hub configurations were slightly changed. Although several brain regions (e.g., the sensorimotor cortex, visual cortex and middle temporal gyrus) were still detected as functional hubs, several regions in the default-mode network were inconspicuous, such as the medial prefrontal cortex in all of the degree maps, and the inferior parietal cortex in the woDeg map. These changes in functional hubs were also observed for the tR-fMRI data without GSR (see Figs. S6B and C). Furthermore, the TRT reliability analysis showed similar spatial maps for three types of degree (Fig. 4B, woDeg vs. wsDeg, r = 0.96; woDeg vs. wlDeg, r = 0.98, all ps < 0.00001, $df_{eff}$s = 5548). Importantly, most brain regions exhibited increased TRT reliability compared with the results of GSR (Fig. 2A). This increasing effect was mostly clear for the lateral temporal areas. Normalized histograms of voxel ICC values for the two regression strategies are displayed in Fig. 4C, which confirmed a higher level of reliability for the analysis without GSR, with approximately the same mean ICC values around 0.46 for all three types of degree.

### Influence of sampling rates on functional hubs

To investigate the influence of sampling rates on functional hubs, we analyzed both the tR-fMRI and mR-fMRI data within the same scan duration (i.e., scan duration = 290 s, which corresponded to the total 116 volumes for tR-fMRI and the first 450 volumes for mR-fMRI).

### Consistency and difference in the spatial patterns of the degree maps

The sparsity of functional networks derived from tR-fMRI and mR-fMRI data was listed in Table 1, and no significant difference was observed between different sampling rates. For each session, the spatial patterns of the functional hubs were highly consistent between tR-fMRI and mR-fMRI (Fig. S7), with high spatial correlation coefficients (≥0.95) for all three types of degree centralities. However, several regions exhibited significantly different short-range degree values at different sampling rates, which were identified using a voxel-wise paired t-test within each session with a corrected p < 0.05 (Figs. 5A and B). Compared with the tR-fMRI data, the mR-fMRI data showed consistently higher weighted short-range degree values in both sessions, which were mainly located in the left medial prefrontal cortex and right middle frontal gyrus (wsDeg, Fig. 5A). These regions were also identified in binary functional networks (bsDeg, Fig. 5B). When considering the
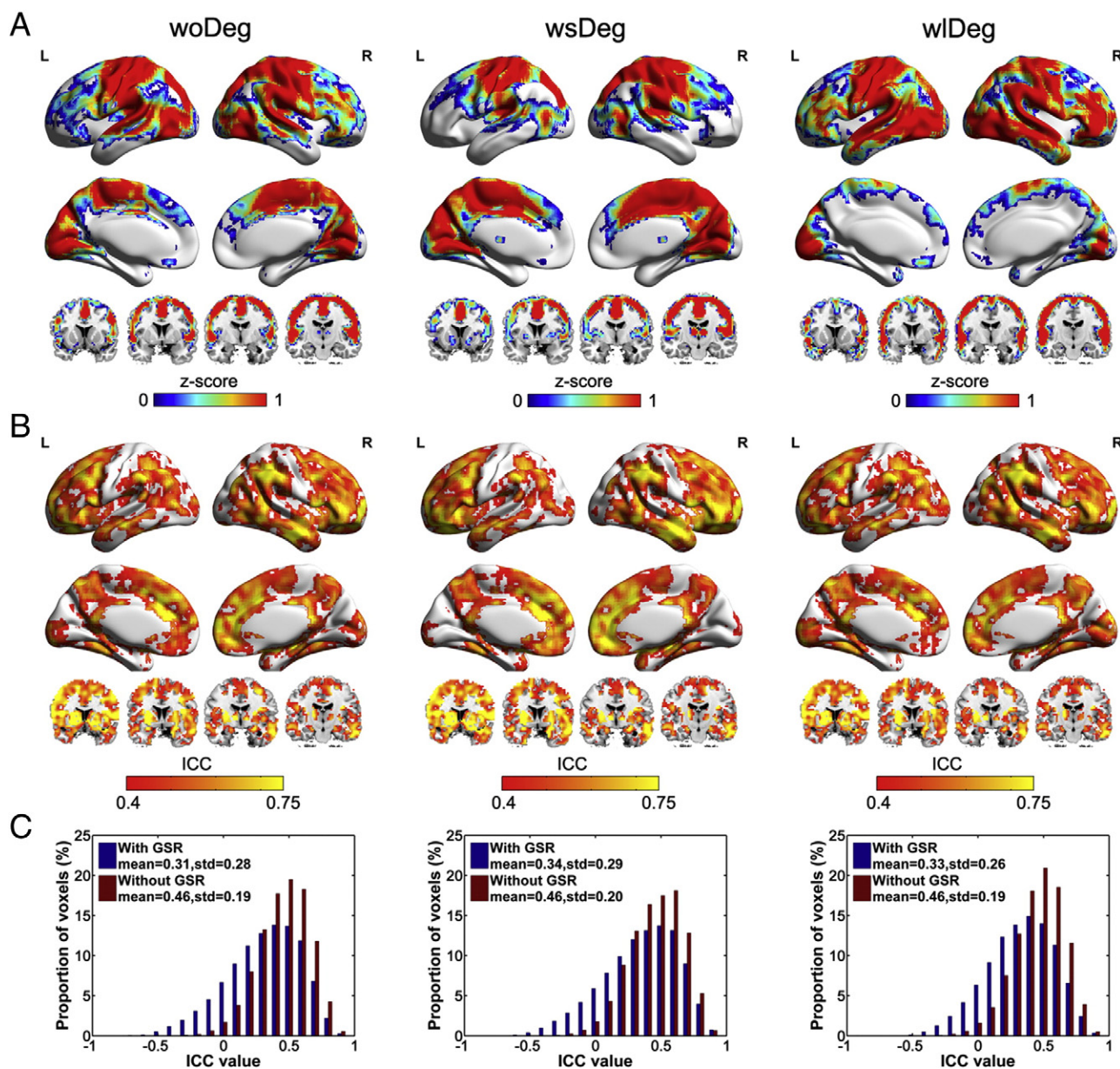
**Fig. 4.** Spatial patterns of functional hubs and their TRT reliability on the basis of the mR-fMRI data without GSR. A, Spatial patterns of functional hubs derived without GSR in session 1. B, TRT reliability maps in the case of without GSR. C, normalized histograms of voxel ICC values in two cases (i.e., with GSR and without GSR). These distributions indicated that the degree centrality exhibited enhanced reliability in the latter case, regardless of the types of degree centralities.

scanning order effects (Fig. 5C), we observed that only a small area of the right lingual gyrus showed significantly different degree values between the two halves of a single mR-fMRI scan for both sessions. These results indicated that the degree differences observed between tR-fMRI and mR-fMRI cannot be explained by the scanning order effects.

*Effects of sampling rates on TRT reliability of degree centrality*

We analyzed the TRT reliability of three types of degree for the tR-fMRI and mR-fMRI data (Figs. 6A and B, woDeg, wsDeg and wlDeg). In general, the spatial patterns of TRT reliability maps were discrepant between different sampling rates with low spatial similarity (tR-fMRI vs. mR-fMRI, woDeg: $r = 0.04$; wsDeg: $r = 0.08$; wlDeg: $r = 0.05$, all ps < 0.05, $df_{eff}s = 5548$). The mean ICC values across the brain were dissimilar for both datasets (tR-fMRI vs. mR-fMRI, woDeg: $0.31 \pm 0.20$ vs. $0.20 \pm 0.30$; wsDeg: $0.27 \pm 0.22$ vs. $0.26 \pm 0.29$; wlDeg: $0.32 \pm 0.21$ vs. $0.17 \pm 0.31$). Most regions exhibited different reliability patterns when the sampling rates changed. The direct contrasts of the reliability maps (mR-fMRI − tR-fMRI) are displayed in

Fig. 6C. We found that several regions, including the posterior medial prefrontal cortex, lateral frontal cortex, right angular gyrus, anterior temporal lobe and paracentral lobule, displayed higher TRT reliability for mR-fMRI, while the lateral temporal lobe and right cuneus exhibited a lower TRT reliability, independent of the type of degree.

*Global hubs in high frequency band functional networks*

We explored the functional hubs and TRT reliability of degree in a high frequency band ($0.2 - 0.3$ Hz), using the whole scan of the mR-fMRI data. Interestingly, this frequency band was not detectable using the tR-fMRI data with TR = 2500 ms. Functional hubs for two sessions are displayed in Figs. 7A and B, respectively, with high spatial similarity (session 1 vs. session2, woDeg: $r = 0.91$; wsDeg: $r = 0.87$; wlDeg: $r = 0.95$, all ps < 0.00001, $df_{eff}s = 5548$). Similar to the regions in the low frequency band ($0.01 - 0.1$ Hz, Fig. 1), some regions in the default-mode network (e.g., medial prefrontal cortex, middle temporal gyrus and inferior parietal lobule) and inferior frontal gyrus were identified as functional hubs. Moreover, the medial and lateral frontal cortex
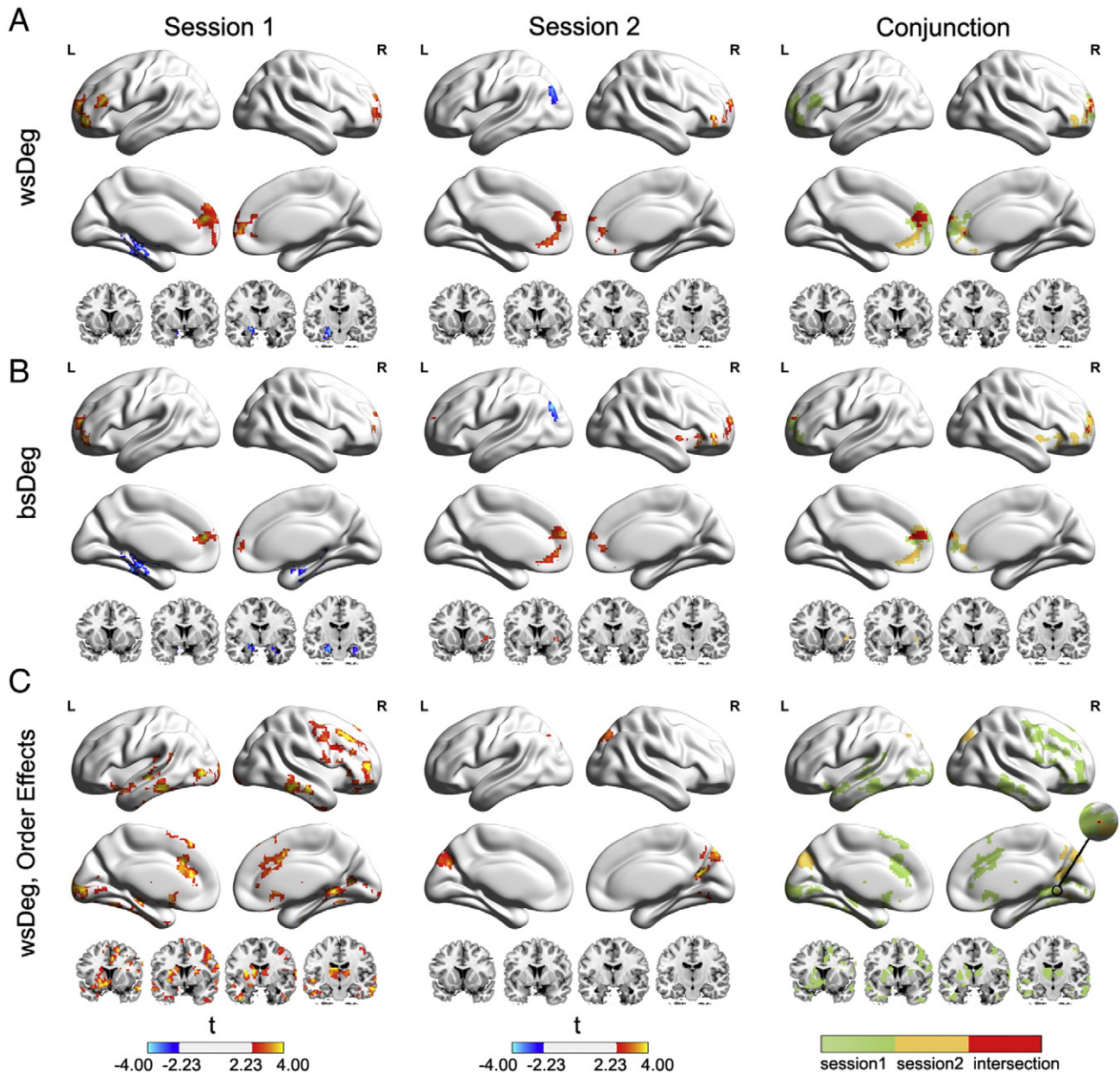
**Fig. 5.** Difference of the short-range degree maps between the mR-fMRI and tR-fMRI data within the same scan duration (290 s). A, difference in the wsDeg maps for both sessions. B, difference in the bsDeg maps for both sessions. Degree maps for tR-fMRI were set as reference in (A) and (B). C, difference in the wsDeg maps between two sections in a single mR-fMRI scan, in order to account for scanning order effects. The corrected t-maps in session 1 and session 2 are shown in the left and middle column, respectively. These t-maps were corrected for multiple comparisons using AlphaSim with a corrected p < 0.05. Conjunctions of corrected positive t-maps for the two sessions are shown in the right column, with inter-section areas of two sessions displayed in red.

was identified without distance-dependence, and the middle temporal gyrus and inferior parietal cortex were evident in the long-range degree maps. In addition, some areas of the cuneus and thalamus were also detected in the short-range degree maps. Furthermore, a large proportion (approximately 65%) of regions across the brain exhibited fair to good reliability (ICC > 0.4) for all three types of degree (Fig. 7C).

*Head motion effects*

Most results showed very few changes after the operation of data scrubbing. For the mR-fMRI data, 10 of the 11 subjects were included after data scrubbing, with 1 subject (subject 4176156) further excluded due to scrubbing 71% of original data. The spatial patterns of the functional hubs and TRT reliability maps in the different conditions were revealed 1) a low frequency band (0.01 − 0.1 Hz) with GSR (Figs. S8 and

S9) and without GSR (Fig. S10), as well as 2) a high frequency band (0.2 − 0.3 Hz) with GSR (Fig. S11). The spatial patterns in these cases were highly similar to previous results (Figs. 1, 2, 4, and 7), but the overall level of TRT reliability was slightly improved in most of the cases after data scrubbing (see more details in Table S2). When directly comparing the degree values of the mR-fMRI and tR-fMRI data, we still found that the regions of left medial prefrontal cortex and right middle frontal gyrus showed a trend (uncorrected p < 0.1, paired t-test) of larger short-range degree values for mR-fMRI data (Fig. S12), which were consistent with the results obtained without scrubbing (Fig. 5).

**Discussion**

This study provides a comprehensive investigation of functional hubs and their test−retest reliability in the voxel-wise human brain
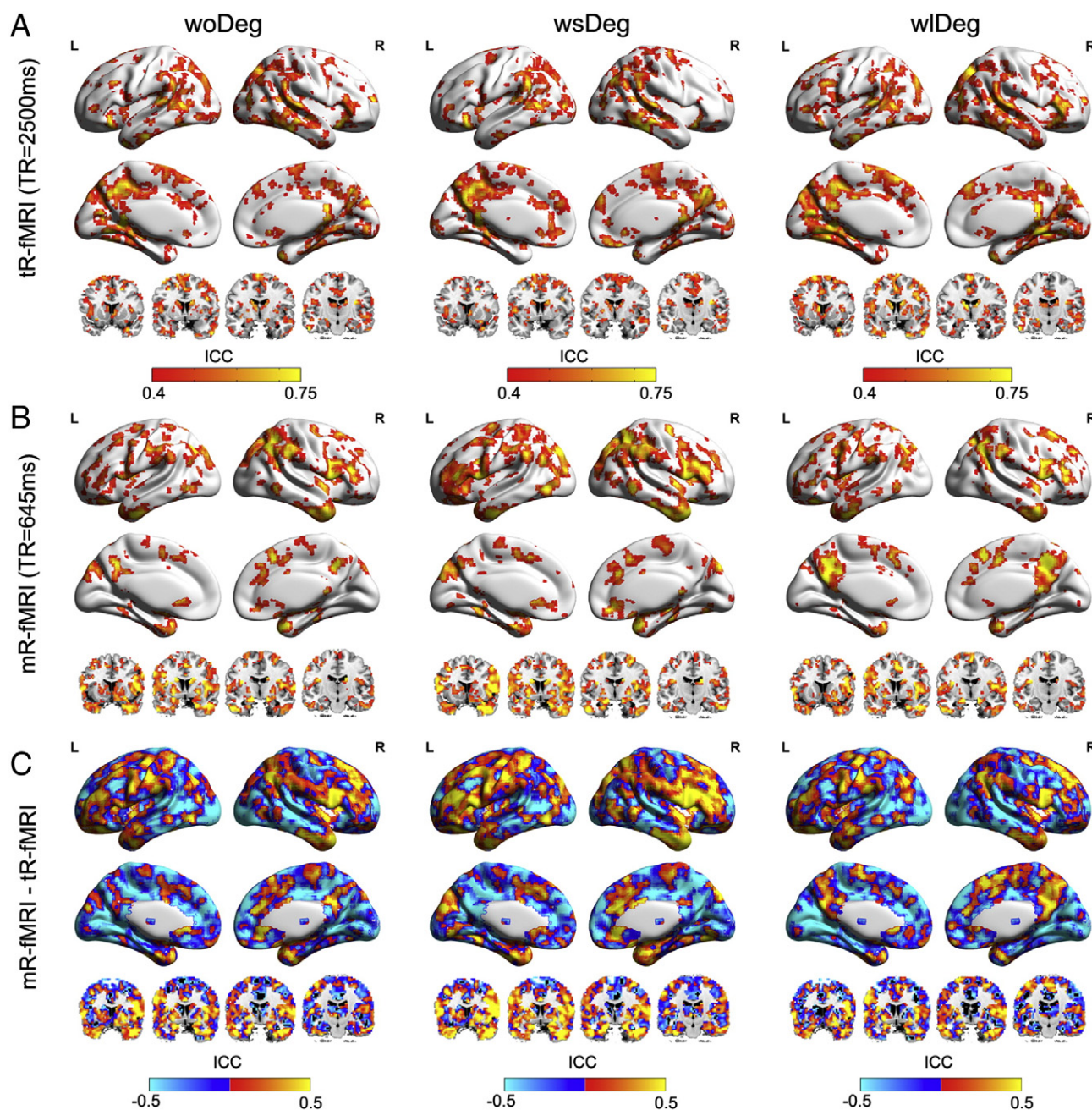
**Fig. 6.** TRT reliability of degree in functional networks derived from the tR-fMRI and mR-fMRI data within the same scan duration (290 s). A, TRT reliability maps for tR-fMRI. B, TRT reliability maps for mR-fMRI. C, direct contrasts of TRT reliability maps are displayed to illustrate the TRT reliability differences between the mR-fMRI and tR-fMRI data. The yellow and blue colors show regions of higher reliability in the mR-fMRI and tR-fMRI data, respectively.

functional networks derived from sub-second multiband R-fMRI scans. The main results are threefold: first, we reproduced previous findings that hub regions were mainly localized at the default-mode regions, sensorimotor and visual cortex. Most hub regions exhibited fair to good TRT reliability, except the cuneus region. Second, we found that the 6-minute mR-fMRI data were able to identify reliable functional hub structures and that the data preprocessing without GSR changed the spatial patterns of functional hubs but improved their TRT reliability. Third, we reported the effect of the sampling rates of R-fMRI scans on functional hubs, and showed the meaningful functional hubs and their TRT reliability in a high frequency band $(0.2 - 0.3 \text{ Hz})$. These results showed very little changes when we further assessed the effect of head motion with data scrubbing. Together, our results suggested the validity of sub-second multiband R-fMRI scans for identifying reliable

functional hubs with the measure of nodal degree centrality. We discuss these findings in more detail in this section.

*Reliable functional hubs in human whole-brain functional networks*

Based on mR-fMRI data, voxel-wise functional brain networks with sparse connections were constructed for each subject, indicating the low wiring-cost of functional network organization (Bullmore and Sporns, 2012). Meanwhile, using the measure of degree centrality, we identified functional hubs that contained large numbers of functional connections, irrespective of scanning time (two sessions, Fig. 1) and sampling rates of R-fMRI scans (Fig. S7). Even in a high frequency band $(0.2 - 0.3 \text{ Hz})$, several hub regions in the default-mode network were still identified (Fig. 7). Consistent with previous studies (Achard
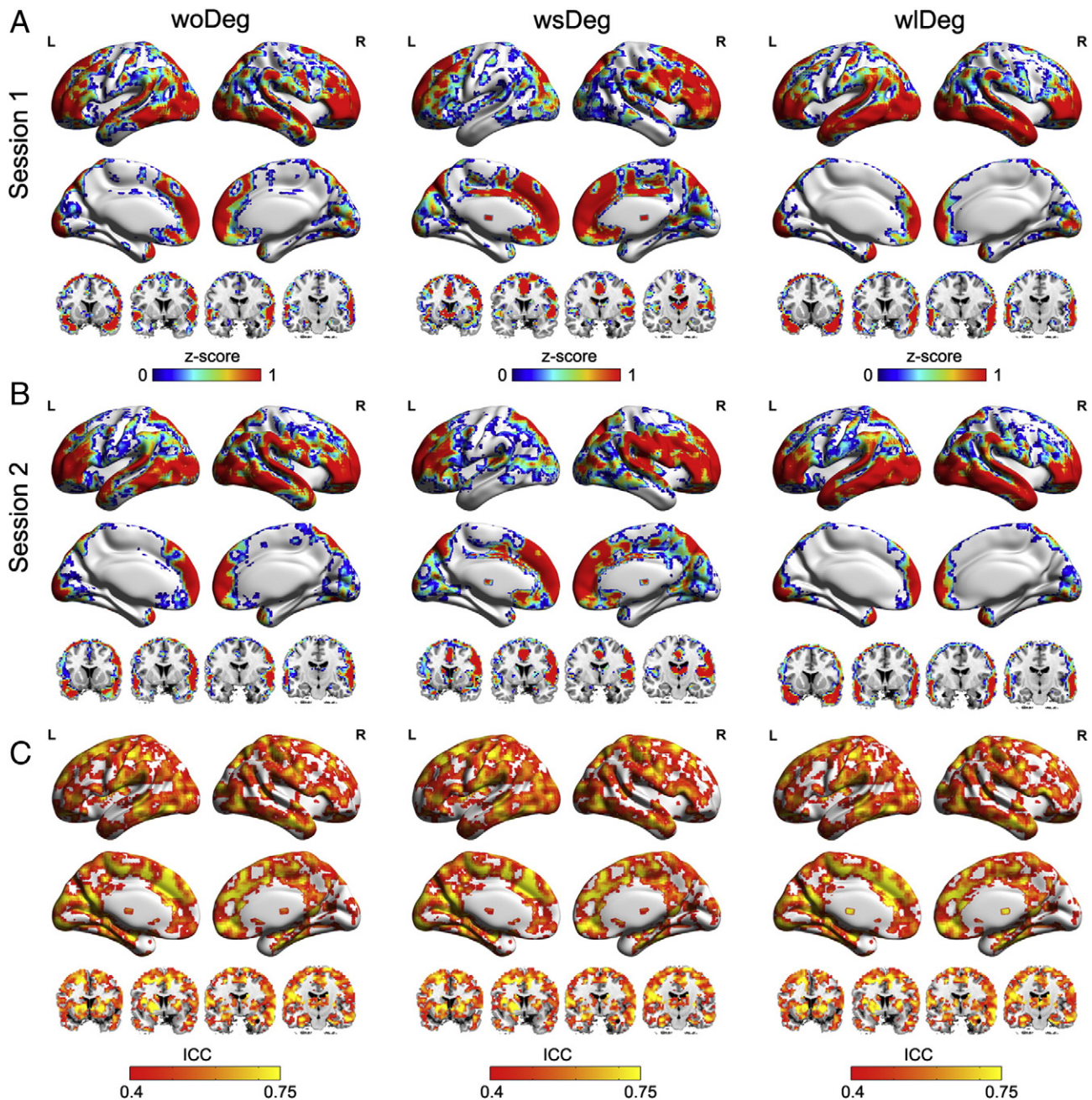
**Fig. 7.** Spatial patterns of functional hubs and their TRT reliability in high-frequency functional networks. A, spatial patterns of functional hubs in session 1. B, spatial patterns of functional hubs in session 2. The spatial patterns of functional hubs were consistent between the two sessions. C, TRT reliability maps for three types of degree centralities (woDeg, wsDeg and wlDeg). The entire scan of the mR-fMRI data was temporally band-pass filtered with a high frequency band (0.2–0.3 Hz).

et al., 2006; Buckner et al., 2009; He et al., 2009; Liang et al., 2013; Sepulcre et al., 2010; Tomasi and Volkow, 2011; Zuo et al., 2012), we identified functional hubs in the voxel-based brain networks. These functional hubs are crucial for efficient information exchange and integration across distributed brain regions. Furthermore, we showed that the distribution of hub regions was anatomically distance-dependent: several primary and sensory association cortices, including the sensorimotor, visual regions and superior parietal lobule, were identified as short-range hubs; whereas, several default-mode and multimodal association cortical areas integrating information from multiple perspective and cognitive areas were identified as long-range hub regions. This pattern was highly consistent with that of recent studies on the basis of traditional R-fMRI data (Liang et al., 2013; Sepulcre et al., 2010). In

particular, the medial prefrontal cortex displayed high levels of both local and distant connectivities, which might reflect its crucial role in processing and transporting sensory information and cognitive control (Sepulcre et al., 2010).

Reliable network metrics are necessary for basic and clinical research (Deuker et al., 2009; Guo et al., 2012). In voxel-wise functional networks derived from mR-fMRI, we found that the TRT reliability maps of degree were spatially non-homogeneous and were moderate across the brain, which was consistent with the previous results (Liang et al., 2012; Wang et al., 2011; Zuo et al., 2012). In addition, most hub regions exhibited fair to good TRT reliability of degree, particularly for some areas within the default-mode network (e.g., precuneus, ventromedial prefrontal gyrus and inferior parietal

cortex), which suggested a potential relationship between TRT reliability of degree and high functional connections as reported previously (Wang et al., 2011). Taken together, our results indicate that the mR-fMRI technique was valid in detecting reliable functional hub configurations in the human whole-brain functional networks with the measure of degree centrality.

### Effects of scan duration

Exploring the effects of scan duration on the reliability of graph metrics is important when using R-fMRI scans to infer convincing results, particularly in populations that show difficulty in keeping still during the scans (e.g., Alzheimer's disease and schizophrenia). Using traditional R-fMRI scans, several studies have explored the effects of different scan durations (5 − 15 min) on the brain's functional connectivity (Van Dijk et al., 2010; Whitlow et al., 2011). For example, Whitlow et al. (2011) reported that functional correlations stabilized after 5 min of R-fMRI scan duration (TR = 2000 ms). In this study, we showed similar results for the nodal degree centrality derived from traditional R-fMRI data (TR = 2500 ms), as shown by the fluctuation increasing of TRT reliability with a scan duration ranging from 1 min to 5 min (Fig. S5). For the mR-fMRI scans with a higher sampling rate (TR = 645 ms), a 6-minute scan duration was able to characterize the brain's functional hub structure. The TRT reliability of degree increased minimally by extending the scan duration beyond 6 min, which was consistent with previous findings with typical sampling rates (Van Dijk et al., 2010). This result could be attributable to the tradeoff of several factors introduced by high sampling rates, such as the additional temporal information regarding functional integrity among brain regions (Smith et al., 2012; Zahneisen et al., 2011), increased degrees of freedom and reduced signal-to-noise ratio (Feinberg et al., 2010). Our finding of the short scan duration was crucial because it demonstrated that multiband R-fMRI scans are feasible and efficient for reliable functional hub analysis, and may provide some references for future studies regarding the functional connections based on mR-fMRI data.

### Effects of global signals

Using the mR-fMRI data, we found that the regression strategy of the global signals affected the spatial configuration of the functional hubs. This finding might have resulted from the spatially non-homogeneous changes of the degree, induced by different correlation distributions relevant to the regression strategies used (Schwarz and McGonigle, 2011). As described in previous studies, network analysis without GSR reduced the anti-correlations among the brain regions (Murphy et al., 2009; Schwarz and McGonigle, 2011; Weissenbacher et al., 2009), which resulted in the increase of degree values. These effects were most obvious in several primary cortical regions, such as the sensorimotor cortex and cuneus. However, a previous study (Liang et al., 2012) reported approximately consistent functional hubs for data preprocessing with and without GSR in brain networks derived from an anatomically defined atlas. This discrepancy could be due to different spatial scales of node definition (i.e., 90 nodes representing brain areas in Liang et al. (2012), compared with 44,401 nodes representing voxels in our analysis). The large number of nodes in our study may have made the changes of degree values much more sensitive to the processing of GSR. Furthermore, we observed that nuisance regression without GSR resulted in a positive contribution on the TRT reliability of degree, and this observation is in accordance with previous results using traditional sampling rates (Guo et al., 2012; Liang et al., 2012). In addition, we found that the positive contribution on TRT reliability was spatially non-homogeneous. Because the physiological source of the global signals is still unclear (Fox et al., 2009; Murphy et al., 2009), the validity of the global signal regression in fMRI studies still requires further studies.

### Effects of sampling rates

We showed consistent anatomically distance-dependent functional hub configurations for the mR-fMRI and tR-fMRI data within the same scan duration, indicating that the functional hubs actually reflect the intrinsic organization characteristics of the brain independent of the different sampling rates. Moreover, most of the regions displayed no significant difference in the degree values between the data with different sampling rates, except in some regions (e.g., left medial prefrontal cortex) (Fig. 5). This discrepancy could be due to the experimental noise, fluctuations of mental states and different types of subject movement. Nevertheless, common significant regions emerged in both sessions around one week apart and these regions exhibited a similar trend after further head motion correction with data scrubbing, implying that these degree differences might mainly result from the superiority of mR-fMRI in temporal resolution. On the one hand, subtle fluctuations of BOLD signals can be acquired, and additional temporal information regarding the underlying neuronal processes might be revealed (Smith et al., 2012; Zahneisen et al., 2011). On the other hand, the effects of undesirable high frequency noises, particularly the respiration signals (~0.3 Hz), might be better reduced via the temporal band-pass filter (0.01–0.1 Hz) for mR-fMRI (Cordes et al., 2001; Lowe et al., 1998; van den Heuvel and Pol, 2010). Further TRT reliability analysis revealed spatially dissimilar reliability maps for mR-fMRI and tR-fMRI data, and the differences were clear in regions of the posterior medial prefrontal cortex, lateral frontal gyrus, paracentral lobule and anterior temporal lobe. This discrepancy between the reliability maps could be associated with the functional connection differences between mR-fMRI and tR-fMRI data in both sessions, and more evidence is required to elucidate the physiological mechanism underlying these reliability differences. Besides, the experiment measurement errors of R-fMRI scans may also have a potential impact on the TRT reliability difference between different sampling rates. However, in the current study we did not take into account these factors, as the measurement errors of both R-fMRI scans were not available. The potential impact of measurement errors could be handled in future reliability analyses, when relevant information is available.

### Functional hubs in a high frequency band

Most previous studies on resting-state functional networks focused on the spontaneous fluctuations of BOLD signals in a low frequency band (0.01–0.1 Hz) (Biswal et al., 2010; Fox and Raichle, 2007; van den Heuvel and Pol, 2010), which may reflect the endogenous coordination of neural activities in the brain (Biswal et al., 1995; Cordes et al., 2000; Lowe et al., 1998). However, less attention has been given to the functional connections in the high frequency band (Achard et al., 2006; Salvador et al., 2005b; Wu et al., 2008), whose physiological mechanism is still unclear. Using mR-fMRI, we were able to construct voxel-wise functional networks in a high frequency band (0.2–0.3 Hz) and to identify some hub regions that were mainly in several default-mode regions (e.g., medial prefrontal cortex and inferior parietal cortex). These delicate spatial patterns of functional hubs suggested that these hubs may not solely originate from thermal (spatially uncorrelated) noises, and therefore, might actually reflect the functional organization of the human brain in the high frequency band. Given that these default-mode regions have been linked to multiple internally-generated mental activity (e.g., mind wandering) (Buckner et al., 2008; Raichle and Snyder, 2007), these findings suggest that the integration of multiple perceptive and cognitive processes might involve functional coordination across a wide frequency band.

### Methodological considerations

Several issues need to be further considered when interpreting our findings. First of all, to exclude the potential effects of confounding

healthy issues, we employed the data of 11 healthy subjects in this study. To increase the statistical power of TRT reliability analysis (e.g., scan duration effects), future studies need to be conducted on a large number of healthy subjects. Second, the effect of head motion on functional connectivity has gained increasing attention, and several methods have been proposed for head motion correction on voxel time courses (Power et al., 2012; Satterthwaite et al., 2013; Van Dijk et al., 2012). In the present study, only the method of data scrubbing (Power et al., 2012) was used to further reduce the effects of head motion on functional connectivity after the nuisance regression with six head motion parameters. The effect of other methods (e.g., regression with high-order head motion related changes) on functional hubs and their TRT reliability will be explored in further work. Third, we observed the discrepancies in the short-range degree maps between the mR-fMRI and tR-fMRI data. These discrepancies might be associated with the different sampling rates that were used between the datasets. However, these results may have also been affected by the order effects of the scan sequences. In the current study, we assess the scanning order effects by dividing a single mR-fMRI scan into two sections with approximately equal scan duration. Nevertheless, to effectively reduce the order effects on the network analysis, it will be important to perform a counter-balance design in future studies. Fourth, we only explored the brain's functional hubs and their TRT reliability in the voxel-based brain networks. Further studies are needed to explore other global network metrics, such as characteristic path length, small-world parameters, and modularity, which provides additional information on the functional network organization (Bullmore and Sporns, 2009; Rubinov and Sporns, 2010). Finally, when monitoring longitudinal changes, it is important to consider the tradeoff between reliability and sensibility of network metrics (Bassett et al., 2011; Deuker et al., 2009; Guo et al., 2012). In future studies, several measures (e.g., the coefficient of variation) can be further developed to comprehensively characterize the sensibility of functional network metrics over scanning sessions.

Supplementary data to this article can be found online at http://dx.doi.org/10.1016/j.neuroimage.2013.07.058.

## Acknowledgments

## Conflict of interest

None.

## References

Achard, S., Salvador, R., Whitcher, B., Suckling, J., Bullmore, E., 2006. A resilient, low-frequency, small-world human brain functional network with highly connected association cortical hubs. J. Neurosci. 26, 63–72.

Alexander-Bloch, A.F., Vertes, P.E., Stidd, R., Lalonde, F., Clasen, L., Rapoport, J., Giedd, J., Bullmore, E.T., Gogtay, N., 2013. The anatomical distance of functional connections predicts brain network topology in health and schizophrenia. Cereb. Cortex 23, 127–138.

Bassett, D.S., Brown, J.A., Deshpande, V., Carlson, J.M., Grafton, S.T., 2011. Conserved and variable architecture of human white matter connectivity. NeuroImage 54, 1262–1279.

Birn, R.M., Diamond, J.B., Smith, M.A., Bandettini, P.A., 2006. Separating respiratory-variation-related fluctuations from neuronal-activity-related fluctuations in fMRI. NeuroImage 31, 1536–1548.

Biswal, B., Yetkin, F.Z., Haughton, V.M., Hyde, J.S., 1995. Functional connectivity in the motor cortex of resting human brain using echo-planar MRI. Magn. Reson. Med. 34, 537–541.

Biswal, B.B., Mennes, M., Zuo, X.N., Gohel, S., Kelly, C., Smith, S.M., Beckmann, C.F., Adelstein, J.S., Buckner, R.L., Colcombe, S., Dogonowski, A.M., Ernst, M., Fair, D., Hampson, M., Hoptman, M.J., Hyde, J.S., Kiviniemi, V.J., Kotter, R., Li, S.J., Lin, C.P., Lowe, M.J., Mackay, C., Madden, D.J., Madsen, K.H., Margulies, D.S., Mayberg, H.S., McMahon, K., Monk, C.S., Mostofsky, S.H., Nagel, B.J., Pekar, J.J., Peltier, S.J., Petersen, S.E., Riedl, V., Rombouts, S.A., Rypma, B., Schlaggar, B.L., Schmidt, S., Seidler, R.D., Siegle, G.J., Sorg, C., Teng, G.J., Veijola, J., Villringer, A., Walter, M., Wang, L., Weng, X.C., Whitfield-Gabrieli, S., Williamson, P., Windischberger, C., Zang, Y.F., Zhang, H.Y., Castellanos, F.X., Milham, M.P., 2010. Toward discovery science of human brain function. Proc. Natl. Acad. Sci. U. S. A. 107, 4734–4739.

Braun, U., Plichta, M.M., Esslinger, C., Sauer, C., Haddad, L., Grimm, O., Mier, D., Mohnke, S., Heinz, A., Erk, S., Walter, H., Seiferth, N., Kirsch, P., Meyer-Lindenberg, A., 2012. Test–retest reliability of resting-state connectivity network characteristics using fMRI and graph theoretical measures. NeuroImage 59, 1404–1412.

Buckner, R.L., Andrews-Hanna, J.R., Schacter, D.L., 2008. The brain's default network. Ann. N. Y. Acad. Sci. 1124, 1–38.

Buckner, R.L., Sepulcre, J., Talukdar, T., Krienen, F.M., Liu, H., Hedden, T., Andrews-Hanna, J.R., Sperling, R.A., Johnson, K.A., 2009. Cortical hubs revealed by intrinsic functional connectivity: mapping, assessment of stability, and relation to Alzheimer's disease. J. Neurosci. 29, 1860–1873.

Bullmore, E., Sporns, O., 2009. Complex brain networks: graph theoretical analysis of structural and functional systems. Nat. Rev. Neurosci. 10, 186–198.

Bullmore, E., Sporns, O., 2012. The economy of brain network organization. Nat. Rev. Neurosci. 13, 336–349.

Cordes, D., Haughton, V.M., Arfanakis, K., Wendt, G.J., Turski, P.A., Moritz, C.H., Quigley, M.A., Meyerand, M.E., 2000. Mapping functionally related regions of brain with functional connectivity MR imaging. Am. J. Neuroradiol. 21, 1636–1644.

Cordes, D., Haughton, V.M., Arfanakis, K., Carew, J.D., Turski, P.A., Moritz, C.H., Quigley, M.A., Meyerand, M.E., 2001. Frequencies contributing to functional connectivity in the cerebral cortex in "resting-state" data. Am. J. Neuroradiol. 22, 1326–1333.

Dai, Z., Yan, C., Wang, Z., Wang, J., Xia, M., Li, K., He, Y., 2012. Discriminative analysis of early Alzheimer's disease using multi-modal imaging and multi-level characterization with multi-classifier (M3). NeuroImage 59, 2187–2195.

Deuker, L., Bullmore, E.T., Smith, M., Christensen, S., Nathan, P.J., Rockstroh, B., Bassett, D.S., 2009. Reproducibility of graph metrics of human brain functional networks. NeuroImage 47, 1460–1468.

Feinberg, D.A., Moeller, S., Smith, S.M., Auerbach, E., Ramanna, S., Gunther, M., Glasser, M.F., Miller, K.L., Ugurbil, K., Yacoub, E., 2010. Multiplexed echo planar imaging for sub-second whole brain FMRI and fast diffusion imaging. PLoS One 5, e15710.

Fox, M.D., Raichle, M.E., 2007. Spontaneous fluctuations in brain activity observed with functional magnetic resonance imaging. Nat. Rev. Neurosci. 8, 700–711.

Fox, M.D., Snyder, A.Z., Vincent, J.L., Corbetta, M., Van Essen, D.C., Raichle, M.E., 2005. The human brain is intrinsically organized into dynamic, anticorrelated functional networks. Proc. Natl. Acad. Sci. U. S. A. 102, 9673–9678.

Fox, M.D., Zhang, D., Snyder, A.Z., Raichle, M.E., 2009. The global signal and observed anticorrelated resting state brain networks. J. Neurophysiol. 101, 3270–3283.

Greicius, M.D., Kiviniemi, V., Tervonen, O., Vainionpää, V., Alahuhta, S., Reiss, A.L., Menon, V., 2008. Persistent default-mode network connectivity during light sedation. Hum. Brain Mapp. 29, 839–847.

Guo, C.C., Kurth, F., Zhou, J., Mayer, E.A., Eickhoff, S.B., Kramer, J.H., Seeley, W.W., 2012. One-year test-retest reliability of intrinsic connectivity network fMRI in older adults. NeuroImage 61, 1471–1483.

He, Y., Wang, J., Wang, L., Chen, Z.J., Yan, C., Yang, H., Tang, H., Zhu, C., Gong, Q., Zang, Y., Evans, A.C., 2009. Uncovering intrinsic modular organization of spontaneous brain activity in humans. PLoS One 4, e5226.

Horovitz, S.G., Fukunaga, M., de Zwart, J.A., van Gelderen, P., Fulton, S.C., Balkin, T.J., Duyn, J.H., 2008. Low frequency BOLD fluctuations during resting wakefulness and light sleep: a simultaneous EEG-fMRI study. Hum. Brain Mapp. 29, 671–682.

Kelly, C., Biswal, B.B., Craddock, R.C., Castellanos, F.X., Milham, M.P., 2012. Characterizing variation in the functional connectome: promise and pitfalls. Trends Cogn. Sci. 16, 181–188.

Liang, X., Wang, J.H., Yan, C.G., Shu, N., Xu, K., Gong, G.L., He, Y., 2012. Effects of different correlation metrics and preprocessing factors on small-world brain functional networks: a resting-state functional MRI study. PLoS One 7, e32766.

Liang, X., Zou, Q., He, Y., Yang, Y., 2013. Coupling of functional connectivity and regional cerebral blood flow reveals a physiological basis for network hubs of the human brain. Proc. Natl. Acad. Sci. U. S. A. 110, 1929–1934.

Lowe, M., Mock, B., Sorenson, J., 1998. Functional connectivity in single and multislice echoplanar imaging using resting-state fluctuations. NeuroImage 7, 119–132.

Moeller, S., Yacoub, E., Olman, C.A., Auerbach, E., Strupp, J., Harel, N., Uğurbil, K., 2010. Multiband multislice GE-EPI at 7 tesla, with 16-fold acceleration using partial parallel imaging with application to high spatial and temporal whole-brain fMRI. Magn. Reson. Med. 63, 1144–1153.

Murphy, K., Birn, R.M., Handwerker, D.A., Jones, T.B., Bandettini, P.A., 2009. The impact of global signal regression on resting state correlations: are anti-correlated networks introduced? NeuroImage 44, 893–905.

Opsahl, T., Agneessens, F., Skvoretz, J., 2010. Node centrality in weighted networks: generalizing degree and shortest paths. Soc. Networks 32, 245–251.

Power, J.D., Barnes, K.A., Snyder, A.Z., Schlaggar, B.L., Petersen, S.E., 2012. Spurious but systematic correlations in functional connectivity MRI networks arise from subject motion. NeuroImage 59, 2142–2154.

Raichle, M.E., Snyder, A.Z., 2007. A default mode of brain function: a brief history of an evolving idea. NeuroImage 37, 1083–1090.

Rubinov, M., Sporns, O., 2010. Complex network measures of brain connectivity: uses and interpretations. NeuroImage 52, 1059–1069.

Salvador, R., Suckling, J., Coleman, M.R., Pickard, J.D., Menon, D., Bullmore, E., 2005a. Neurophysiological architecture of functional magnetic resonance images of human brain. Cereb. Cortex 15, 1332–1342.

Salvador, R., Suckling, J., Schwarzbauer, C., Bullmore, E., 2005b. Undirected graphs of frequency-dependent functional connectivity in whole brain networks. Phil. Trans. R. Soc. B 360, 937–946.

Sampat, M., Whitman, G., Stephens, T., Broemeling, L., Heger, N., Bovik, A., Markey, M., 2006. The reliability of measuring physical characteristics of spiculated masses on mammography. Br. J. Radiol. 79, S134–S140.

Satterthwaite, T.D., Elliott, M.A., Gerraty, R.T., Ruparel, K., Loughead, J., Calkins, M.E., Eickhoff, S.B., Hakonarson, H., Gur, R.C., Gur, R.E., Wolf, D.H., 2013. An improved framework for confound regression and filtering for control of motion artifact in the preprocessing of resting-state functional connectivity data. NeuroImage 64, 240–256.

Schwarz, A.J., McGonigle, J., 2011. Negative edges and soft thresholding in complex network analysis of resting state functional connectivity data. NeuroImage 55, 1132–1146.

Sepulcre, J., Liu, H., Talukdar, T., Martincorena, I., Yeo, B.T., Buckner, R.L., 2010. The organization of local and distant functional connectivity in the human brain. PLoS Comput. Biol. 6, e1000808.

Shrout, P.E., Fleiss, J.L., 1979. Intraclass correlations: uses in assessing rater reliability. Psychol. Bull. 86, 420–428.

Smith, S.M., Miller, K.L., Moeller, S., Xu, J.Q., Auerbach, E.J., Woolrich, M.W., Beckmann, C.F., Jenkinson, M., Andersson, J., Glasser, M.F., Van Essen, D.C., Feinberg, D.A., Yacoub, E.S., Ugurbil, K., 2012. Temporally-independent functional modes of spontaneous brain activity. Proc. Natl. Acad. Sci. U. S. A. 109, 3131–3136.

Tomasi, D., Volkow, N.D., 2011. Functional connectivity hubs in the human brain. NeuroImage 57, 908–917.

van den Heuvel, M.P., Pol, H.E.H., 2010. Exploring the brain network: a review on resting-state fMRI functional connectivity. Eur. Neuropsychopharmacol. 20, 519–534.

Van Dijk, K.R.A., Hedden, T., Venkataraman, A., Evans, K.C., Lazar, S.W., Buckner, R.L., 2010. Intrinsic functional connectivity as a tool for human connectomics: theory, properties, and optimization. J. Neurophysiol. 103, 297–321.

Van Dijk, K.R., Sabuncu, M.R., Buckner, R.L., 2012. The influence of head motion on intrinsic functional connectivity MRI. NeuroImage 59, 431–438.

Wang, J.H., Zuo, X.N., Gohel, S., Milham, M.P., Biswal, B.B., He, Y., 2011. Graph theoretical analysis of functional brain networks: test–retest evaluation on short- and long-term resting-state functional MRI data. PLoS One 6, e21976.

Wang, J., Zuo, X., Dai, Z., Xia, M., Zhao, Z., Zhao, X., Jia, J., Han, Y., He, Y., 2013. Disrupted functional brain connectome in individuals at risk for Alzheimer's disease. Biol. Psychiatry 73, 472–481.

Weissenbacher, A., Kasess, C., Gerstl, F., Lanzenberger, R., Moser, E., Windischberger, C., 2009. Correlations and anticorrelations in resting-state functional connectivity MRI: a quantitative comparison of preprocessing strategies. NeuroImage 47, 1408–1416.

Whitlow, C.T., Casanova, R., Maldjian, J.A., 2011. Effect of resting-state functional MR imaging duration on stability of graph theory metrics of brain network connectivity. Radiology 259, 516–524.

Wu, C.W., Gu, H., Lu, H., Stein, E.A., Chen, J.-H., Yang, Y., 2008. Frequency specificity of functional connectivity in brain networks. NeuroImage 42, 1047–1055.

Xia, M., Wang, J., He, Y., 2013. BrainNet viewer: a network visualization tool for human brain connectomics. PLoS ONE 8, e68910.

Xiong, J., Gao, J.H., Lancaster, J.L., Fox, P.T., 2004. Clustered pixels analysis for functional MRI activation studies of the human brain. Hum. Brain Mapp. 3, 287–301.

Yan, C., Zang, Y., 2010. DPARSF: a MATLAB toolbox for "pipeline" data analysis of resting-state fMRI. Front. Syst. Neurosci. 4, 13.

Yeo, B.T., Krienen, F.M., Sepulcre, J., Sabuncu, M.R., Lashkari, D., Hollinshead, M., Roffman, J.L., Smoller, J.W., Zöllei, L., Polimeni, J.R., 2011. The organization of the human cerebral cortex estimated by intrinsic functional connectivity. J. Neurophysiol. 106, 1125–1165.

Zahneisen, B., Grotz, T., Lee, K.J., Ohlendorf, S., Reisert, M., Zaitsev, M., Hennig, J., 2011. Three-dimensional MR-encephalography: fast volumetric brain imaging using rosette trajectories. Magn. Reson. Med. 65, 1260–1268.

Zar, J.H., 1996. Biostatistical Analysis. Prentice Hall, Upper Saddle River, NJ.

Zhang, J., Wang, J., Wu, Q., Kuang, W., Huang, X., He, Y., Gong, Q., 2011. Disrupted brain connectivity networks in drug-naive, first-episode major depressive disorder. Biol. Psychiatry 70, 334–342.

Zuo, X.N., Ehmke, R., Mennes, M., Imperati, D., Castellanos, F.X., Sporns, O., Milham, M.P., 2012. Network centrality in the human functional connectome. Cereb. Cortex 22, 1862–1875.

Zuo, X.N., Xu, T., Jiang, L., Yang, Z., Cao, X.Y., He, Y., Zang, Y.F., Castellanos, F.X., Milham, M.P., 2013. Toward reliable characterization of functional homogeneity in the human brain: preprocessing, scan duration, imaging resolution and computational space. NeuroImage 65, 374–386.